PHILOSOPHICAL TRANSACTIONS A

Phil. Trans. R. Soc. A.
doi:10.1098/not yet assigned

MULTI-PHASE PERMITTIVITY IMAGING USING ABSOLUTE VALUE ELECTRICAL CAPACITANCE TOMOGRAPHY DATA AND A LEVEL SET ALGORITHM

E Al Hosani, M Soleimani*

Engineering Tomography Lab (ETL), Electronic & Electrical Engineering, University of Bath, Bath, UK

Keywords: Electrical Capacitance Tomography (ECT), multi-phase flow imaging, multiple level set reconstruction, absolute capacitance data.

Abstract: Multi-phase flow imaging is a very challenging and critical topic in industrial process tomography. In this article, simulation and experimental results of reconstructing the permittivity profile of multi-phase material from data collected in Electrical Capacitance Tomography (ECT) are presented. A multi-phase narrowband level set algorithm is developed to reconstruct the interfaces between three or four phase permittivity values. The level set algorithm is capable of imaging multi-phase permittivity by using one set of ECT measurement data, so called absolute value ECT reconstruction and this is tested with high contrast and low contrast multiphase data. Simulation and experimental results showed the superiority of this algorithm over classical pixel based image reconstruction methods. Multi-phase level set algorithm and absolute ECT reconstruction are presented for the first time in this paper and critically evaluated.

1 INTRODUCTION

Multiphase flows that appear in many industries (i.e oil and gas, aerospace, chemicals, etc) are considered complex and unpredictable. Sometimes a multiphase flow is combined with undesirable deposits and dirt (which are considered as another phase) that disturb the system and defect instrumentations. In order to ensure safety and increase profits, the multiphase flow must be adequately controlled [1]. In order to do so, an analysis of the multiphase flow is required to determine some of the flow feature/properties such as the flow regime, number of phases, concentration of each phase, etc. Currently the multiphase flow is being analysed by means of a) Multi-Phase Flow Meters (MPFM) to get the flow rate of each phase or b) process tomography to get an image of the cross section of the actual pipe under process. Each method has its limitations and being constantly enhanced and modified. A comprehensive review of the different process tomography techniques was conducted by [2].

Electrical Capacitance Tomography (ECT) is one method of process tomography used in industrial process monitoring for imaging the cross-section of a pipe/vessel. It measures the external capacitance of the enclosed objects to determine the internal permittivity distribution, which is then used to reconstruct an image

*Author for correspondence (M.Soleimani@bath.ac.uk).

of the process. ECT was first developed in the late 1980's to image a two-phase flow [3]. Afterwards, ECT systems were used successfully in numerous research investigations for industrial multi-phase processes including gas/solid distribution in pneumatic conveyors [4], fluidized beds [5-7], flame combustion [8-10], gas/liquid flows [11], water/oil/gas separation process [12], water hammer [13], determining the characteristic of the molten metal in Lost Foam Casting process [14], deposit detection [15] and many others. This paper presents a new application area for ECT as a novel imaging technique and measurement tool for multiphase flows in pipelines. The method presented here demonstrates the ability and potential of ECT imaging for multi-phase flow imaging and measurement using absolute ECT data.

Most studies for process ECT employ classical iterative reconstruction techniques, where the inverse problem is solved iteratively by updating the estimated model thus improving the match between the measured and the calculated capacitance. However, such iterative techniques require stabilization, thus a least squares functional is usually augmented by some additional regularization terms. Such regularization may lead to 'over-smoothing' the reconstructed images, which makes the characterization of all different phases in terms of size and contrast a major challenge, especially when one of the phases has low concentration or has relatively higher permittivity. The interaction between the capacitance measurements and the process media is nonlinearly influenced by the inhomogeneity of the flow. Accordingly, applying standard reconstruction that is based on regularization tools usually only result in low-resolution images, especially in high contrast cases where one phase has higher permittivity value compared to the other phases. This makes classical reconstruction techniques more challenging in terms of correctly distinguishing the other low permittivity phases since the high permittivity phase will dominate and make the problem highly nonlinear. Thus, so far the ECT system is mainly used to image a low contrast non-conductive media such, not taking into consideration the more complicated scenarios of a multiphase media. However, some conductive medias, such as water-continuous flow in oil pipelines, are being recently investigated with different conditions.

In this paper, a multiphase shape reconstruction based on level set method for ECT is presented, where the multiphase framework for image segmentation developed by [16] and the narrowband level set formulation developed by [17] are modified and employed to tackle this non-linear problem. Both high and low contrast cases of a multiphase reconstruction are studies. In this approach, the permittivity values of all different phases are approximated and assumed to be known while their size, shape, and location are recovered from the data. The aim of our reconstruction is to correctly determine the location of the present phases and their concentration. This is done by estimating the size and contrast of every phase without an emphasis on the exact shape of the phases but rather an estimated one. The multiphase level set shape reconstruction results shown in this paper are some of the first ones using experimental data of ECT. Such information has the potential to be used for Multi-Phase Flow Metering (MPFM).

In this paper, section 2 introduces the ECT system, section 3 describes the image reconstruction method used and developed whereas section 4 shows some simulated and experimental results of the low and high

contrast cases. Section 5 gives an analysis of the results and explains the superiority of our method over classical pixel based reconstruction methods.

2 ECT SYSTEM

Fig. 1 shows a typical 12 electrodes ECT system, which comprises mainly of three subsystems; the capacitance sensor, the data acquisition unit and the computer unit. The capacitance sensor consists of more than one electrode, an external shield, and axial and radial guards as seen in Fig1 (a). Typically, several electrodes are mounted equidistantly on the periphery of the non-conductive object to be imaged (i.e process pipe or vessel). The adjacent electrodes are separated from each other by a small piece of copper called the axial guard. In order to reduce external electrical noise, eliminate the effects of external grounded objects, and protect the electrodes from damages, a screen is used to cover the electrodes, which can be either conductive or non-conductive. An insulating material is used to fill the gap between the electrodes and the screen. To reduce the standard capacitance between adjacent electrode pairs, the sensor also includes radial guards. The screen and the radial guards are always maintained at earth potential. Different configurations of the radial and axial guards were proposed and studied to improve the system performance.

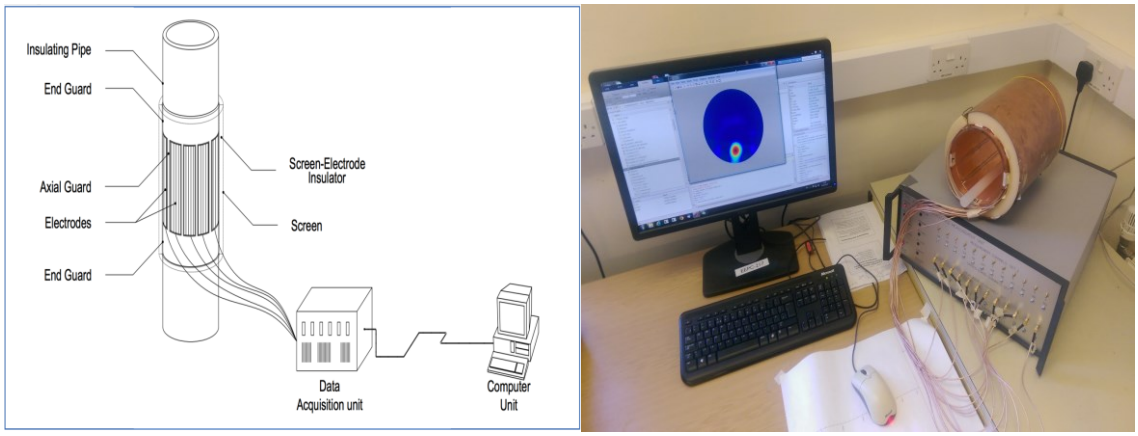

(a) (b)

Figure 1. The ECT system (a) schematic of the ECT system (b) ECT system of the University of Bath Engineering Tomography Lab.

Numerous measurement protocols can be used for an *N* electrode system. However, in a typical ECT system, electrodes 1 to *N* are used consecutively as source electrodes, and the capacitance values amongst all pair combinations are measured. This means that for one measurement cycle of a 12-electrode ECT sensor, electrode 1 will first act as the source electrode after being excited with a fixed positive voltage whereas electrodes 2 to 12 will act like the detectors by being held at earth potential. Afterwards, the capacitances between 1-2, 1-3, …, 1-12 are measured concurrently using transducers. Next, electrode 2 will act as the source electrode and electrodes 3 to 12 act as the detectors, while electrode 1 will be inactive to eliminate reciprocity. This process continues until electrode 11 acts as the source electrode and only electrode 12 acts as the detector,

while electrodes 1 to 10 are inactive. Commonly, the number of independent capacitance measurements M is given by the number of N-electrode combinations, taking 2 at a time as $\mathrm{M} = \frac{N(N-1)}{2}$.

The data acquisition unit measures and conditions the signals that are acquired from the capacitance sensor. The data acquisition unit works according to the following sequence of events:

1. Apply a fixed voltage, V_c, to the source electrode while keeping the rest of the detectors grounded.
2. Measure the induced currents in the detectors and their capacitive components by the use of phase sensitive detector.
3. Deduce the capacitance measurements C from the given potential difference V_c and the measured current Q according to $C = \frac{Q}{V}$.
4. Convert the capacitance measurements into voltage signals using a capacitance to voltage converter.
5. Condition (i.e multiplex, amplify, filter, …etc.) and digitalize the voltage signals.
6. Send the conditioned and digitalized voltage signals to a computer for further processing and display.

The computer unit receives the voltage signals from the data acquisition unit and interprets them again into capacitance measurements in order to use them for the image reconstruction algorithm to determine the permittivity distribution (i.e the image). The measured capacitance values C between a source electrode i and a detector j can be represented in a matrix as:

$$\boldsymbol{C_{i,j}} = \begin{bmatrix} \boldsymbol{C_{1,2}} & \boldsymbol{C_{1,3}} & \dots & \boldsymbol{C_{1,N}} \\ & \boldsymbol{C_{2,3}} & \dots & \boldsymbol{C_{2,N}} \\ & & \ddots & \vdots \\ & & & \boldsymbol{C_{N-1,N}} \end{bmatrix} \boldsymbol{for} \begin{pmatrix} \boldsymbol{i = 1, \dots, N-1} \\ \boldsymbol{j = i+1, \dots, N} \end{pmatrix} \qquad (1)$$

3 IMAGE RECONSTRUCTION

3.1 The Forward Problem

The ECT forward problem needs to be solved before solving the ECT inverse problem. The ECT mathematical system model can be modelled by Poisson's equation as it can be treated as an electrostatic field problem. Assuming no free charge within the field, Poisson's equation can be simplified to Laplace's equation:

$$\boldsymbol{\nabla . \left(\varepsilon_o \varepsilon \, (x, y) \, \nabla u(x, y) \right) = 0} \qquad (2)$$

where ε_o is the free space permittivity, $\varepsilon \, (x, y)$ and $u(x, y)$ are the 2D permittivity distribution and the electrical potential distribution respectively. Laplace's equation is solved with the following Dirichlet boundary conditions:

$$\boldsymbol{u^i} = \begin{cases} \boldsymbol{V_c} & \forall(\boldsymbol{x},\boldsymbol{y}) \subseteq \boldsymbol{\Gamma_i} \quad \boldsymbol{where}\ (\boldsymbol{i = 1, \dots, N-1}) \\ \boldsymbol{0} & \forall(\boldsymbol{x},\boldsymbol{y}) \subseteq \boldsymbol{\Gamma_k}(\boldsymbol{k \neq i}),\ \boldsymbol{\Gamma_{guards}}\ \textbf{and}\ \boldsymbol{\Gamma_{screen}} \end{cases} \tag{3}$$

where V_c is a fixed voltage applied to the source electrode, Γ_i is the spatial location of electrode i, Γ_{guards} and Γ_{screen} are the spatial location of the guards and screen respectively. In other words, (3) states that the boundary condition is a fixed voltage V_c applied to the source electrode while the detectors, guards and screen are kept grounded. The measured capacitance can be calculated by

$$\boldsymbol{C_{ij}} = -\frac{\boldsymbol{\varepsilon_o}}{\boldsymbol{V_{ij}}} \int_{\boldsymbol{\Gamma_j}} \boldsymbol{\varepsilon}\,(\boldsymbol{x},\boldsymbol{y})\, \boldsymbol{\nabla u^q}(\boldsymbol{x},\boldsymbol{y}).\, \boldsymbol{\hat{n}}\, \boldsymbol{d\Gamma_j} \qquad \boldsymbol{for} \begin{pmatrix} \boldsymbol{i = 1, \dots, N-1} \\ \boldsymbol{j = i+1, \dots, N} \end{pmatrix} \tag{4}$$

where Γ_j is the surface of the detector and $\hat{n}$ is a unit vector normal to Γ_j and u^q is the electrical potential distribution of node q of the Finite Element Method (FEM) mesh in the detector j. And V_{ij} is the voltage difference between the detector and the source electrode i (i.e $V_i - V_j$). The FEM is used to calculate the capacitance and the sensitivity distribution [15]. This study presents a nonlinear multi-phase level set algorithm, which will work with one capacitance data (i.e absolute capacitance data). In this case the background data of free space is used for a simple scaling calibration of the forward model.

3.2 Level Set Based Inverse Problem

Osher and Setain first developed the level set method in the 1980s for modeling the front propagation of surfaces under curvature. [18]. Since then, it has been used in many disciplines, such as image processing, fluid mechanics, optimal design, computer graphics, computational geometry and inverse problems. Santosa [19] was the first to develop two computational approaches for inverse problems based on the level set method in which the desired unknown is a region in $\mathbb{R}^2$ or $\mathbb{R}^3$. The first approach results in a Hamilton-Jacobi equation, which is nonlinear time-dependent partial differential equation for the level set function whose evolution minimizes the residual in the data fit. Whereas the second approach is based on an optimization method (i.e Gauss-Newton) that generates a sequence of level set functions that reduces the residual. For electrical and electromagnetic tomography in particular, some initial studies were conducted using different types of level set techniques for shape reconstruction (i.e [16, 20-21]).

In level set method, the constructed shapes are given as the zero level set of one or more higher dimensional function called the "level set function". By updating this function the constructed shapes can move accordingly, and thus the topological changes can be performed automatically. Hence, instead of finding $\mathcal{E}_{int}$, the level set technique is able to represent boundaries of different shapes by the zero level set of a predefined level set function ψ. For a 2-dimentional problem, suppose D is the characteristic set of interest. Then the boundary of the inclusion ∂D is the interface between the two materials and is given by the zero level set of the function ψ as:

$$\partial D = \{r : \psi(r) = 0\} \quad (5)$$

Thus, the image parameter at each point, $\varepsilon(r)$ can be represented in terms of a level set function as:

$$\varepsilon(r) = \begin{cases} \mathcal{E}_{int} \; for \{r : \psi(r) < 0\} \\ \mathcal{E}_{ext} \; for \{r : \psi(r) > 0\} \end{cases} \quad (6)$$

Accordingly, the capacitance data can be described as a function of a level set function $C = F(\psi(\varepsilon(r)))$.

Equation (6) represents the mapping that assigns to a given level set function the corresponding permittivity distribution. This can be denoted as $\varepsilon = \varphi(\psi(r))$. Representing the $\varepsilon(r)$ through a level set function $\psi(r)$ instead of representing it in terms of D makes the image reconstruction process simpler, as no *a priori* assumption about the topology (i.e spatial location) or the nature (i.e shape and size) of D is needed. On the other hand, due to the nonlinear dependence of ε on ψ, this approach will lead to a nonlinear inverse problem even if the forward problem was linearized. Notice that in this inverse problem statement, $\varepsilon(r)$ is not the unknown, instead it only perform as an intermediate parameter to arrive at the real unknown, which is the level set function $\psi(r)$.

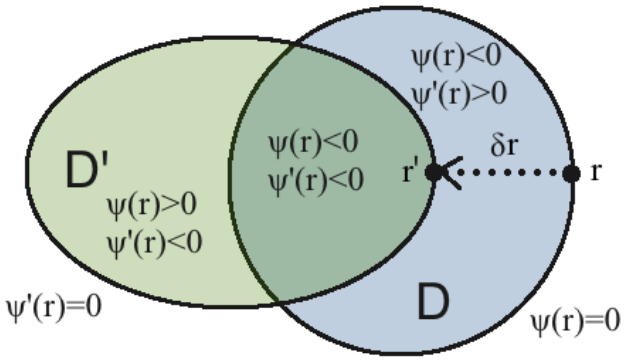

Figure 2. The geometry of the variation of the point $r \to r'$ under a variation of $\psi(r) \to \psi'(r)$

In order to facilitate the dependence of the forward map on small changes on the shape, we look at the variation of ε caused by a variation in ψ. Let r be a point on the boundary of D which is represented by (5). Suppose $\psi(r)$ and r are perturbed by a small variation giving $\psi'(r) = \psi(r) + \delta\psi(r)$ and $r' = r + \delta r$ respectively. This will result in changing the region D to be a new region denoted by D'. Accordingly, ε will vary to $\varepsilon' = \varepsilon + \delta\varepsilon$. In Fig.2 notice that r which was on the boundary of D and on $\psi(r) = 0$ now belongs to $\mathcal{E}_{int}$ of $\psi(r)$ and the boundary of D' ($\psi'(r) = 0$) according to (6). Fig.2 shows how updating the level set function will change the status of each point r to belong to either $\mathcal{E}_{int}$ or $\mathcal{E}_{ext}$ of the new level set $\psi'(r)$,

Equation (6) is suitable for two-phase reconstruction; however, it can be extended to cover multiple phases as several authors have suggested. One of the earliest and most common methods for multiphase image

reconstruction is based on the colour level set technique, which was first proposed by Vese and Chan [16] for image segmentation. In this technique, the evolution of up to 2^p different phases can be described using p level set functions. However, in this study, a modification of the colour level set method suggested by [22] was employed for the ECT reconstruction. In this approach, m different phases are described by using p=m-1 level set functions. Therefore, three level set equations are used to represent four phases (Fig.3) where each of the four phases is allowed to have any complex topology. Accordingly (6) can be extended to be:

$$\varepsilon\,(r) = \begin{cases} \mathcal{E}_1 & for\ \{r:\ \psi_1(r) \le 0\} \\ \mathcal{E}_2 & for\ \{r:\ \psi_1(r) > 0\ and\ \psi_2(r) \le 0\} \\ \mathcal{E}_3 & for\ \{r:\ \psi_1(r) > 0\ and\ \psi_2(r) > 0\ and\ \psi_3(r) \le 0\} \\ \mathcal{E}_4 & for\ \{r:\ \psi_1(r) > 0\ and\ \psi_2(r) > 0\ and\ \psi_3(r) > 0\} \end{cases} \tag{7}$$

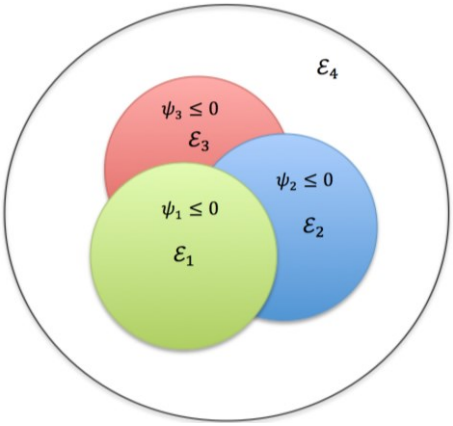

Figure 3. Employed level set representation for representing four different phases (i.e $\mathcal{E}_1, \mathcal{E}_2, \mathcal{E}_3$ and $\mathcal{E}_4$) by three level set functions.

This level set function ψ is given as *a priori* assumption at first and then updated in such a way that moves the boundaries accordingly. Such updates are chosen in a way that reduces a given cost function. One of the first employed techniques for updating moving boundaries is based on a time evolution approach leading to a Hamilton-Jacobi equation. However, another approach for shape reconstruction using level set is the use of optimization methods as an alternative to shape evolution, which was first suggested by Santosa [19]. To find the update of the level set, different optimization techniques can be employed. This study employs a modified optimization approach based on the Gauss-Newton method to derive the updates for the level set function.

In the optimization approach, a sequence of surfaces $\psi_k(r)$ such that $D_k \to D$ where $\partial D_k = \{r:\ \psi(r) = 0\}$ is generated. To solve the inverse problem in a least square sense, the minimizer of the objective functional $J(\varepsilon)$ is found

$$\arg\min_{\psi} J(\psi) = \|F(\psi(\varepsilon\,(r))) - C\|_2^2 + \alpha Reg(\psi(\varepsilon\,(r)) \tag{8}$$

where α>0 is the regularization parameter that can be tuned with different mathematical techniques and $Reg(\psi(\varepsilon\ (r))$ is the regularization term, which is an arbitrary functional that takes different form depending on the regularization method applied, and the argument in the generalized equation can be set according to the requirements of the solution. Different regularization methods have been used to enhance the level set method such as curve shortening [16-17,22]. The regularization term has much less effect on the problem when using a level set method, which makes the problem better posed. Using a modified Gauss-Newton approach for minimizing the nonlinear least squares functional $J(\psi)$ in equation (8) we arrive at the following equation for the level set evolution:

$$\psi\ (\varepsilon)^{k+1} = \psi\ (\varepsilon)^{k} + \xi^{k}(B^{T,k}B^{k}+\alpha^{k}L^{T}L)^{-1}B^{T,k}(F(\psi\ (\varepsilon)^{k}) - C) \qquad (9)$$

With $B = SK$ and $K = c\chi$

where

- L is the regularization matrix. In this paper we considered $L^{T}L = I$, alternatively other regularization matrices can also be used such as Laplacian.
- ξ is the step size (relaxation) parameter, which is the magnitude of change in shape in every update. The step size can stay constant for all alterations or can be changed with the iterations. For this study the step size was chosen by trial and error and was held constant for all iterations.
- B is the narrowband Jacobian matrix, which represents the sensitivity values of only those few elements surrounding ∂D of all different regions.
- S is the sensitivity matrix for all elements of the FEM mesh
- K is the discretised form of $\varepsilon = \varphi\ (\psi(r))$, which includes the indicator function χ of a small narrowband of half width an FEM element centred at ∂D and a constant c as a normalization factor.

As it can be noticed from equation (9), the inverse problem of the interfaces between two different materials is solved using a narrow-band method where only the surrounding pixels are inverted. This technique tends to improve the computational cost and the condition number of the discrete inverse problem by decreasing the number of unknowns compared to the traditional pixel based image reconstruction.

Both the regularization parameter α and the step size parameter ξ need to be tuned in order to arrive at their optimal choice, which depends on the mesh density, the permittivity contrast and the initial guess of the permittivity values. In general, the larger α is chosen, the smoother the updates will be and the harder for the scheme to perform splitting of the topological changes. In this study, α was manually tuned for each case. However, other techniques can be applied to make the reconstruction process more automatic.

The initial guess of the level set functions can be any kind of function, however, the most common choice is a distance function $\psi^{k} = -dist(\partial D)$. In this paper, we choose 3 separated circular inclusions to be the initial guesses for all three level set functions as:

$$\psi^k = (X - X_0)^2 + (Y - Y_0)^2 - \rho^2 \qquad (10)$$

where (X_0, Y_0) are the Cartesian coordinate of the center and ρ is the radius of the circular inclusion. Fig.4 shows a flowchart of the level set ECT image reconstruction algorithm developed for this study.

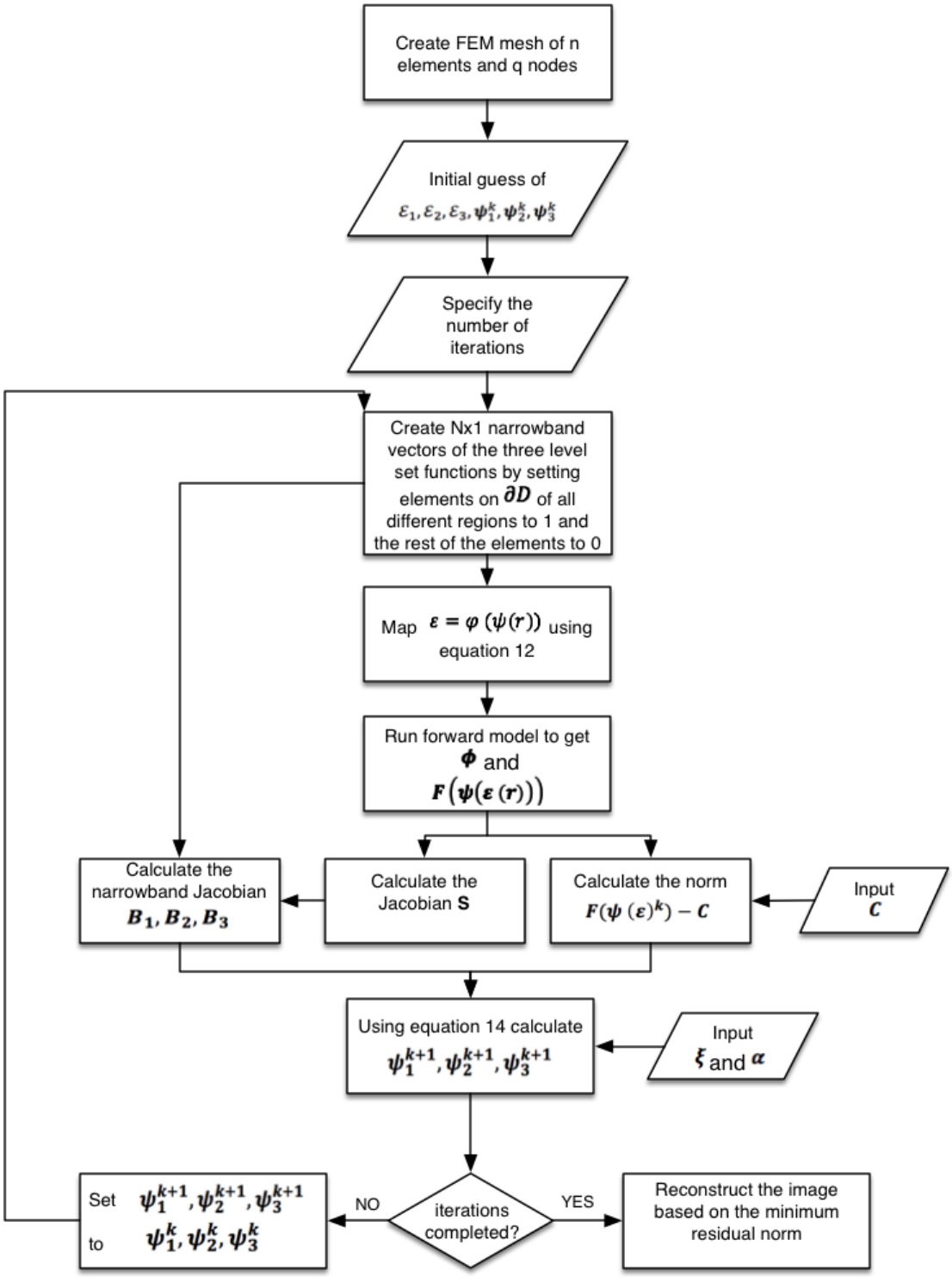

Figure 4. Flowchart of the level set ECT image reconstruction algorithm developed for this study

4 EVALUATION OF MULTIPHASE MONITORING USING LEVEL SET METHOD

To demonstrate the power of this algorithm for multiphase monitoring simulated and experimental results of low contrast and high contrast cases are shown and discussed. For the low contrast case, more than two different phases, which all have low permittivity values are imaged and analysed. This case can be related to real scenarios such as when a pipeline is carrying $\mathcal{E}_1 = gas, \mathcal{E}_2 = oil$ and $\mathcal{E}_3 = low\ permittivity\ deposits$. On the other hand, for the high contrast case, a combination of low permittivity and high permittivity phases are imaged and analysed. This case can be related to real scenarios such as when a pipeline is carrying $\mathcal{E}_1 = gas$, $\mathcal{E}_2 = oil$, $\mathcal{E}_3 = deposits$ and $\mathcal{E}_4 = water$. This case is relatively harder to image using traditional pixel based methods as the inverse problem becomes highly nonlinear when a high permittivity component is introduced as it dominates the region. FEM mesh models were designed and used for the inverse problem, where 1367 three-nod nonhomogeneous triangular elements (i.e pixels) corresponding to 739 nodes were generated to create the mesh.

4.1 Simulation Results

For the sake of comparison, the traditional Tikhonov image reconstruction simulation results for both cases are shown and discussed to illustrate the advantage of the shape based reconstruction methods over the classical pixel based methods.

4.1.1 *Case 1: low contrast simulation*

A 4-phase simulation was conducted and the results for the low contrast case for both the level set method and the standard Tikhonov image reconstruction method are shown in Fig.5 along with the true shape for the sake of comparison. The permittivity values used in the simulation were $\mathcal{E}_1 = 4$, $\mathcal{E}_2 = 3$, $\mathcal{E}_3 = 2$ and $\mathcal{E}_4 = 1$. In order to construct the level set image, 250 iterations were used and the norms of the error between the simulated and calculated capacitances for all iterations are shown in Fig.6. The level set reconstructed image shown in Fig.5 (b) is based on the minimum residual norm, which in this case appeared in iteration 155. This shows that the best result might not occur in the latest iteration, rather somewhere in the iteration process. Accordingly, the algorithm might just terminate at the minimum residual iteration to reduce the computation cost.

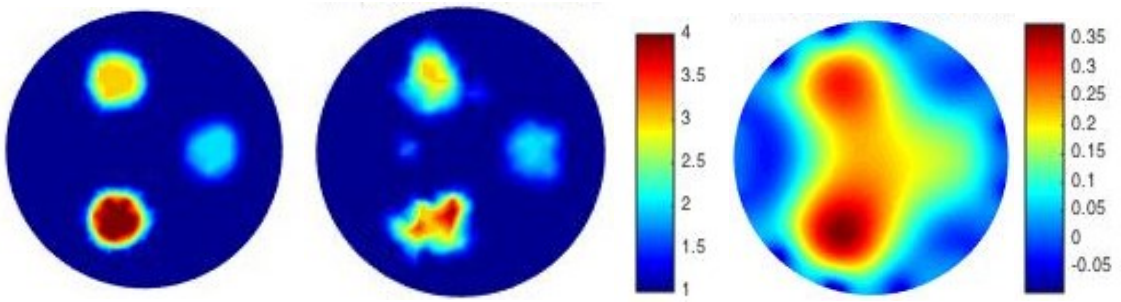

Figure 5. Simulation results for case 1 (a) the true shape of the simulation (b) the reconstructed shape using level set method (c) the reconstructed shape using standard Tikhonov image reconstruction method

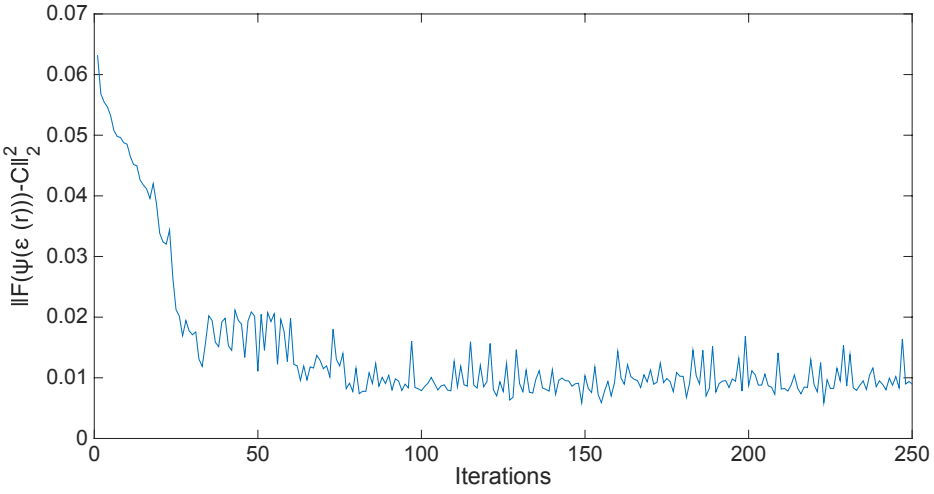

Figure 6. The norms of the error between the simulated and calculated capacitances for 250 iterations of the level set method for case 1.

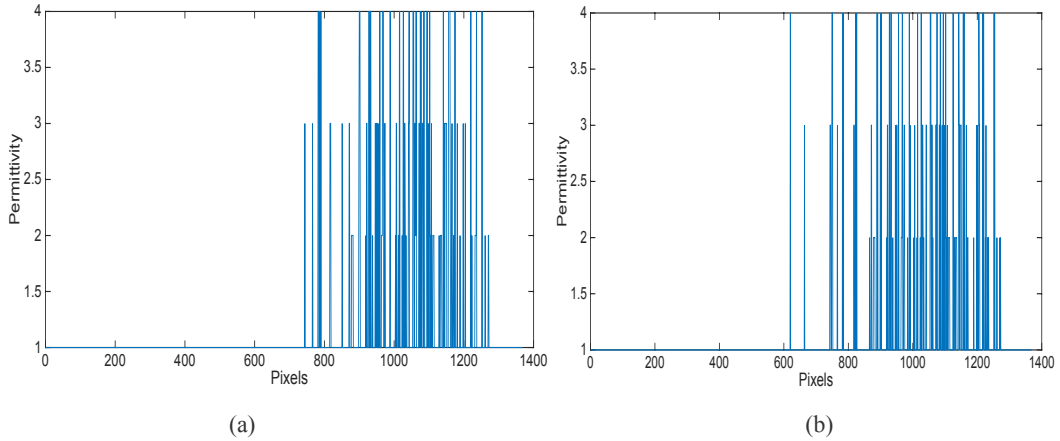

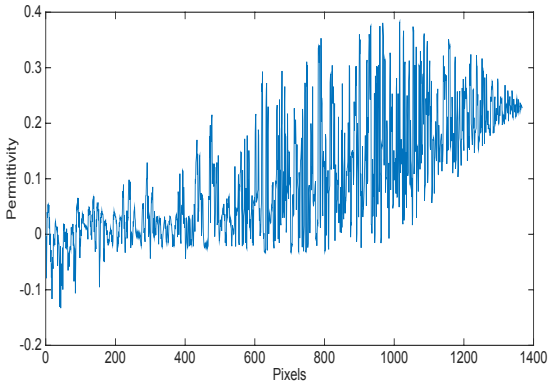

(c)

Figure 7. a histogram of the permittivity distribution per pixel for case 1 (a) true shape, (b) the level set reconstruction, (c) the standard Tikhonov image reconstruction.

Fig.7 shows the histograms of the permittivity distribution per pixel for the true shape, the level set reconstruction and the standard Tikhonov image reconstruction respectively. The obvious similarity between the true shape and the level set reconstruction histograms demonstrate the superiority of the level set method over the traditional Tikhonov reconstruction. The histogram of the level set method shown in Fig.7 (b) shows only 4 phases and each pixel strictly belongs to one and only one of the 4 possible phases. On the other hand the histogram of the standard Tikhonov image reconstruction method shown in Fig.7 (c) shows a large range of permittivity values, which makes such methods harder to threshold and hence information about the individual phases are harder to obtain.

4.1.2 *Case 2: high contrast simulation*

A 4-phase simulation was conducted and the results for the high contrast case for both the level set method and the standard Tikhonov image reconstruction method are shown in Fig.8 along with the true shape for the sake of comparison. The permittivity values used for the 4-phase simulation were $\mathcal{E}_1 = 80, \mathcal{E}_2 = 3, \mathcal{E}_3 = 2$ and $\mathcal{E}_4 = 1$. In order to construct the level set image, 250 iterations were used and the norms of the error between the simulated and calculated capacitances for all iterations are shown in Fig.9. The level set reconstructed image shown in Fig.8 (b) is based on the minimum residual norm, which in this case appeared in iteration 172. Fig.10 shows the histograms of the permittivity distribution per pixel for the true shape, the level set reconstruction and the Tikhonov image reconstruction respectively.

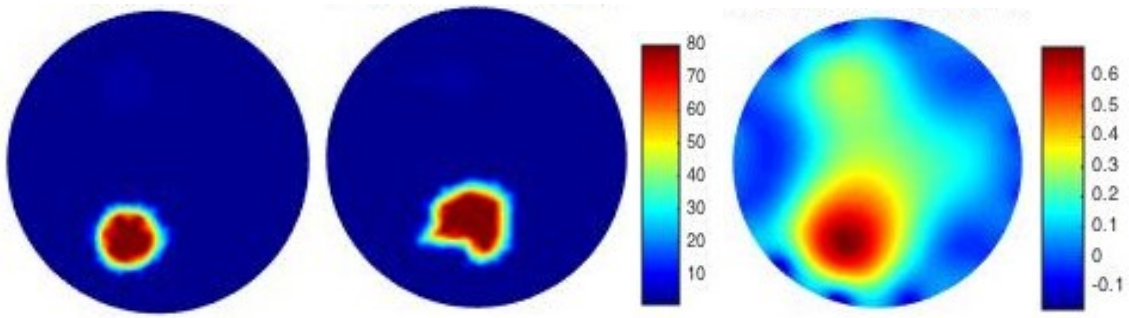

(a) (b) (c)

Figure 8. Simulation results for case 2 (a) the true shape of the simulation (b) the reconstructed shape using level set method (c) the reconstructed shape using standard Tikhonov image reconstruction method

From Fig.8 (a) and (b), it can be seen that the high permittivity phase of water is dominating the region and thus it is hard to see with the bare eye the lower permittivity phases. However, all phases do exist in the data and this is evident by the histograms of the permittivity distribution per pixel shown in Fig.10 (a) and (b). Also, the number of reconstructed pixels per phase was extracted to calculate the phase volume fraction and it is shown in Table.1.

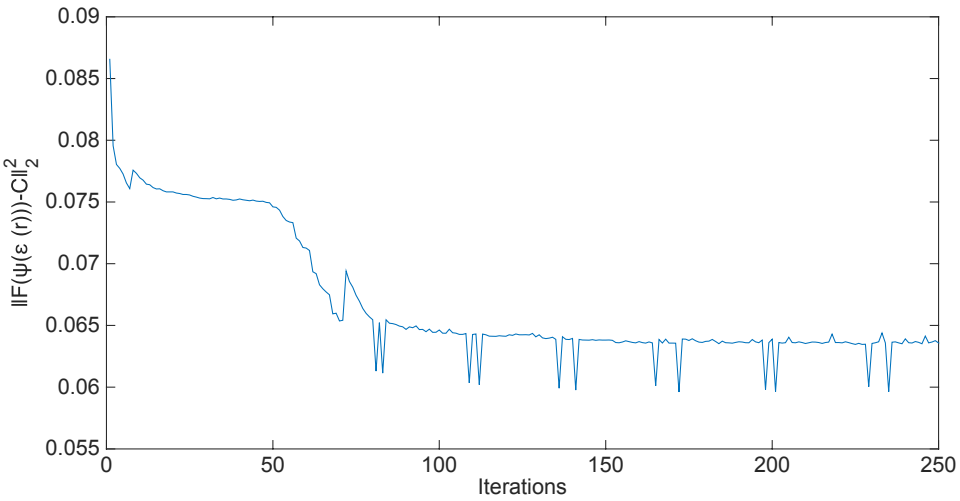

Figure 9. The norms of the error between the simulated and calculated capacitances for 250 iterations of the level set method for case 2.

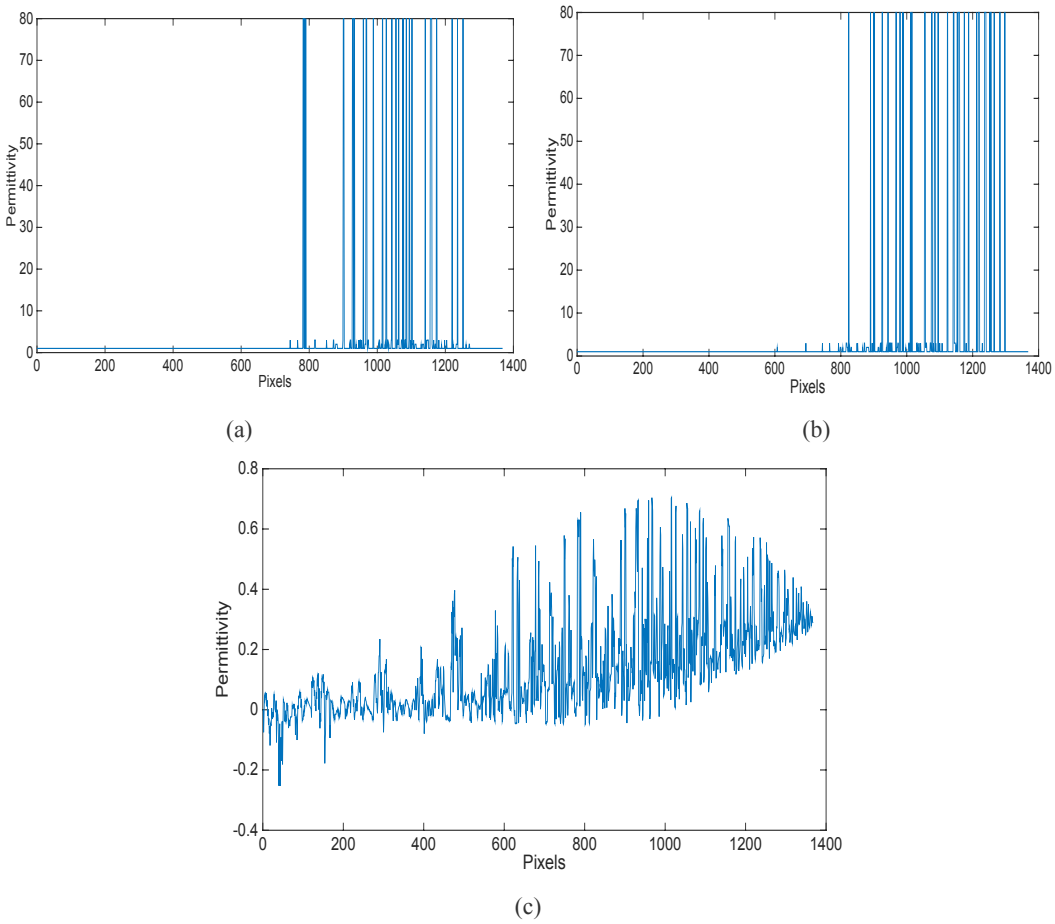

Figure 10. A histogram of the permittivity distribution per pixel for case 2 (a) true shape, (b) the level set reconstruction, (c) the standard Tikhonov image reconstruction.

4.1.3 *Simulated phase area fraction*

By definition, the phase area fraction is the cross-sectional area locally occupied by the phase of a multiphase region, divided by the cross-sectional area of the entire region (e.g pipe) at the same local point. This can be translated digitally by dividing the number of pixels per phase over the total number of pixels. Consequently, the area fractions of all phases were calculated according to the below equation and given in table.1.

$$\text{Phase area fraction} = \frac{number\ of\ pixels\ per\ phase}{total\ number\ of\ pixels} \qquad (11)$$

Table 1. A comparison between the true shape and the level set reconstruction in terms of the area fraction per phase for the simulated cases

	Area Fraction							
	True shape				Level Set reconstruction			
Phase Permittivity	ε_1	ε_2	ε_3	ε_4	ε_1	ε_2	ε_3	ε_4

Case 1:low contrast	0.034	0.033	0.032	0.901	0.027	0.031	0.034	0.909
Case 2:high contrast	0.034	0.033	0.032	0.901	0.044	0.032	0.021	0.903

Calculating the phase area fraction demonstrates the ability of extracting information using ECT by the level set method. The phase fraction is a key parameter for determining other important parameters such as density, viscosity, average velocity, pressure drop, and heat transfer.

4.2 Experimental Results

For the experimental evaluation, a 12-electrode sensor was used, which was built in the University of Bath Engineering Tomography Lab (ETL). The sensor has an inner diameter of 151mm whereas the data acquisition unit used is a commercial PTL300E-TP-G capacitance measurement unit from Process Tomography Limited (Fig. 1.b). The unit can collect sets of capacitance data at 100 frames\s with an effective resolution of 0.1 fF and measurement noise level better than 0.07 fF. MATLAB was used for data collection, image reconstruction and processing. Four different experimental models were prepared in the laboratory in order to examine the ability of the algorithm to detect and distinguish different phases.

4.2.1 *Case 3: low contrast experimental*

The experimental results for the low contrast case for the level set method is shown in Fig.11 along with the experimental setups for the sake of comparison. Two experimental setups were investigated:

- Setup 1: is a 3-phase setup where two wooden rods of permittivity $\mathcal{E}_1 = 2.3$ and a plastic rod of permittivity $\mathcal{E}_2 = 3$ were reconstructed against an air background of permittivity $\mathcal{E}_3 = 1$.
- Setup 2: is a 4-phase setup where a plastic rod of permittivity $\mathcal{E}_1 = 3$ and a wooden rod of permittivity $\mathcal{E}_2 = 2.3$ were divided by a book of permittivity $\mathcal{E}_3 = 3.85$ and reconstructed against an air background of permittivity $\mathcal{E}_4 = 1$. This setup is more challenging since all phases are close in permittivity values and are closely located to each other.

Such simple experimental setups is sufficient for a static study as long as they provide different phases (i.e different permittivity values) and can be considered as a valid first step towards studying multiphase process fluids.

In this case 250 iterations were used to construct the level set image and the norms of the error between the measured and calculated capacitances for all iterations are shown in Fig.12. The level set reconstructed images shown in Fig.11 are based on the minimum residual norm. Standard Tikhonov reconstruction was not produced for the experiment data because absolute capacitance data was used to generate the level set images where only one measured data set was used without the need of a reference data set. Whereas standard Tikhonov

reconstruction needs a reference data set to produce good results. Hence, using standard Tikhonov when absolute data is used could not generate meaningful images.

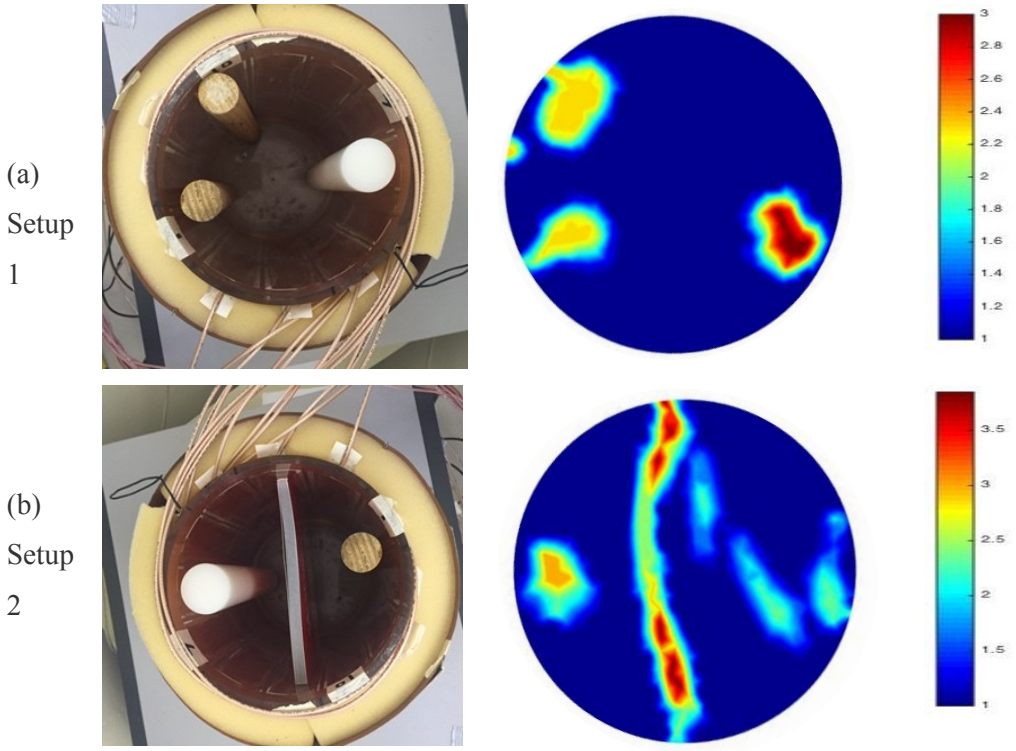

Figure 11 level set experimental results for case 3 (a) experimental setup 1, (b) experimental setup 2.

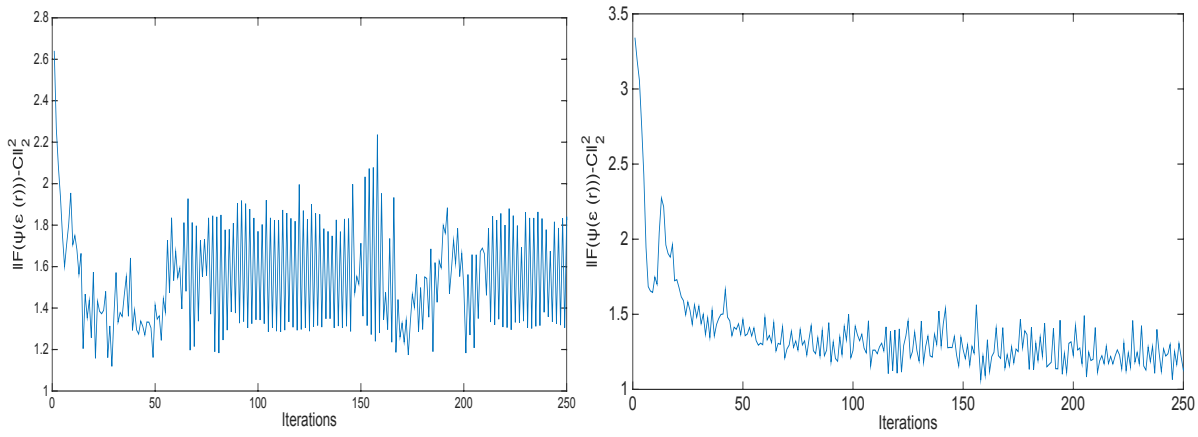

Figure 12. The norms of the error between the measured and calculated capacitances for 250 iterations of the level set method for case 3 (a) experimental setup 1, (b) setup 2.

Fig.13 shows the histograms of the permittivity distribution per pixel. Comparison between the true shape and the level set reconstruction histograms is hard to achieve for experimental setups, however these histogram demonstrate the superiority of the level set method over the traditional Tikhonov reconstruction. This can be seen in the constant permittivity values of the level set method (each constant represents one phase).

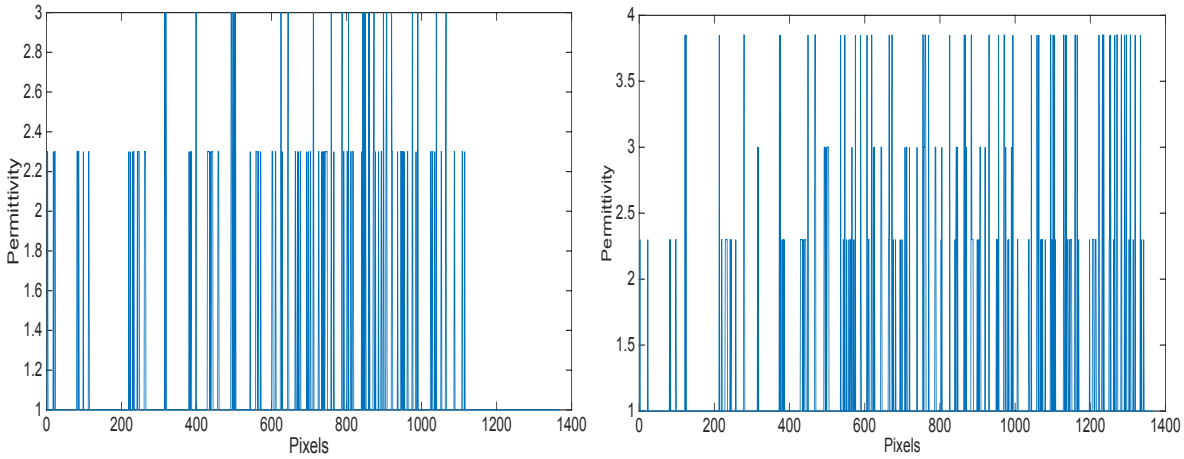

(a) (b)

Figure 13. a histogram of the permittivity distribution per pixel for case 3 (a) experimental setup 1, (b) experimental setup 2.

4.2.2 *Case 4: high contrast experimental*

The experimental results for the high contrast case for the level set method are shown in Fig.14 along with the experimental setups for the sake of comparison. Two setups were investigated:

- Setup 3: is a 3-phase setup where water of permittivity $\mathcal{E}_1 = 80$ (ignoring the plastic thin bottle) and two wooden rods of permittivity $\mathcal{E}_2 = 2.3$ were reconstructed against an air background of permittivity $\mathcal{E}_3 = 1$.
- Setup 4: is a 4-phase setup where water of permittivity $\mathcal{E}_1 = 80$, a plastic rod of permittivity $\mathcal{E}_2 = 3$ and two wooden rods of permittivity $\mathcal{E}_3 = 2.3$ were reconstructed against an air background of permittivity $\mathcal{E}_4 = 1$. This setup is more challenging since wood and plastic are close in permittivity values and are closely located to each other.

In this case 250 iterations were used to construct the level set images and the norms of the error between the measured and calculated capacitance for all iterations are shown in Fig.15. The level set reconstructed images shown in Fig.14 are based on the minimum residual norm. Since water with its high permittivity is dominating the area, it is hard to distinguish the lower permittivity phases from the reconstructed images. However, the number of pixels per phase can be extracted as seen in the histogram (Fig.16) of the permittivity distribution per pixel. Accordingly, the phase area fraction can be extracted and analysed as in table 2.

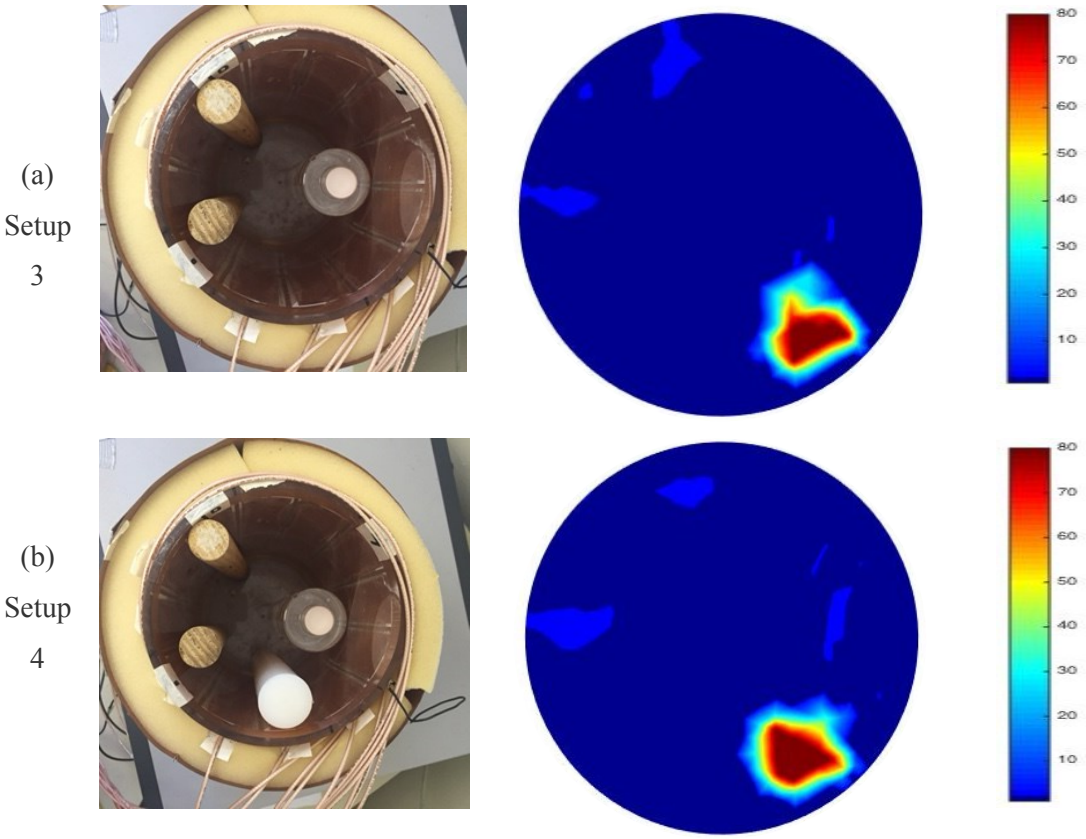

Figure 14 level set experimental results for case 4 (a) experimental setup 3, (b) experimental setup 4.

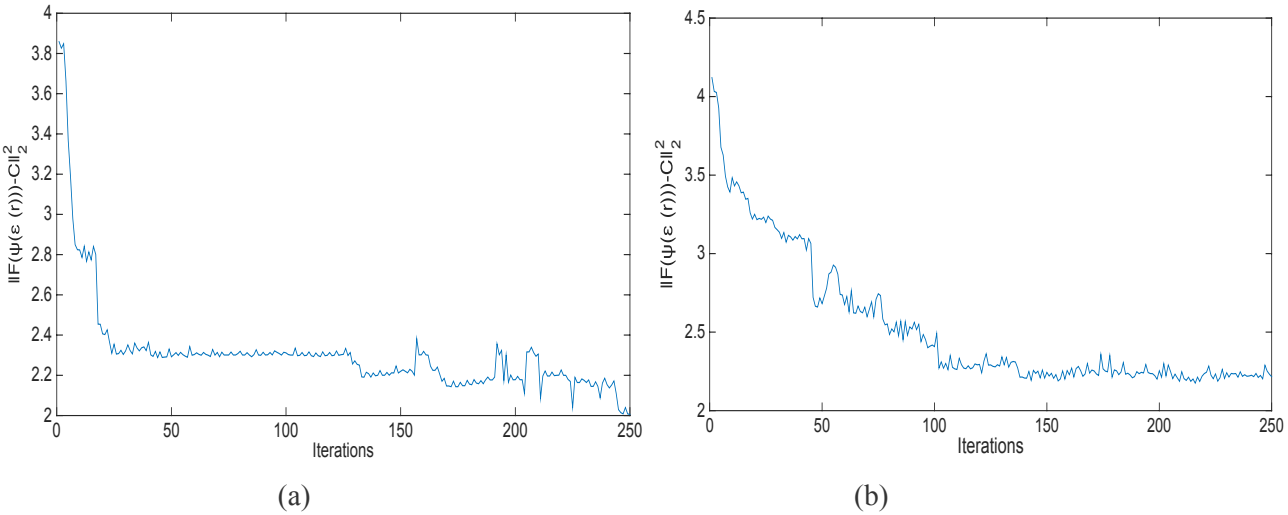

Figure 15. The norms of the error between the measured and calculated capacitances for 250 iterations of the level set method for case 4 (a) experimental setup 3, (b) setup 4.

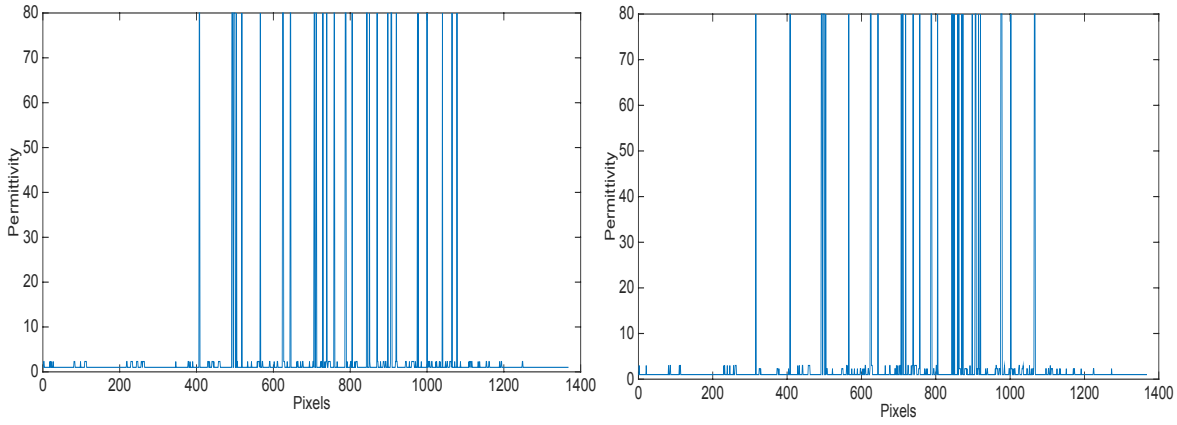

(a) (b)

Figure 16. a histogram of the permittivity distribution per pixel for case 4 (a) experimental setup 3, (b) experimental setup 4.

4.2.3 *Experimental phase area fraction*

The area fractions of all phases for the level set reconstruction of the experimental cases were calculated according to 11 and given in table.2. For the true shape (experimental setup) area fraction, the following equation was used:

$$\text{Phase area fraction (for experemental setup)} = \frac{phase\ cross\ sectional\ area}{pipe\ cross\ sectional\ area} \qquad (12)$$

Table 2. A comparison between the true shape and the level set reconstruction in terms of the area fraction per phase for the experimental cases

	Area Fraction							
	True shape				Level Set reconstruction			
Phase Permittivity	ε_1	ε_2	ε_3	ε_4	ε_1	ε_2	ε_3	ε_4
Case 3: low contrast setup 1	0.054	0.025	0.921	NA	0.084	0.032	0.884	NA
Case 3: low contrast setup 2	0.025	0.027	0.080	0.868	0.031	0.081	0.051	0.836
Case 4: high contrast setup 3	0.032	0.054	0.914	NA	0.042	0.091	0.867	NA
Case 4: high contrast setup 4	0.032	0.025	0.054	0.889	0.048	0.069	0.042	0.841

5 DISCUSSION

One objective of this study is to demonstrate the ability of the level set method to detect and quantify all phases despite any pre knowledge. From the results, it can be seen that this objective can be better achieved by the level set method than traditional regularization based image reconstruction. This can be observed from the reconstructed level set images, which show similar patterns of the true patterns shown in the simulated and experimental results. Another advantage of the level set shape reconstruction method over traditional MPFMs is the ability to accurately estimate the phase volume fraction, as illustrated in table.1 and 2. This is because unlike traditional MPFMs, the level set method does not require any *a priori* information except for the permittivity values of each phase.

The results shown in this paper are designed in order to study the potential of this algorithm for multiphase imaging. The algorithm shows promising results, however it is also open for enhancement. The performance of this method and hence the accuracy can be further investigated and enhanced by refining the following features:

- Generally, the permittivity values may be known and supplied to the algorithm as *a priori* assumption, but methods can be extended where both the permittivity values and the topology are determined simultaneously [23].
- A pre-step of determining the best initial guess of the level set functions can improve the speed of convergence.
- The level set model can be improved by modifying the number/type of used level set functions and/or the mapping $\varepsilon = \varphi\ (\psi(r))$ shown in (7).
- The tuning parameters (i.e the step size, the regularization parameter) and the regularization matrix can be chosen differently using other methods to arrive at the best choices.
- In order to adapt this method to online monitoring, the tuning parameters can be automated.
- Applying a less dense mesh or stopping the iteration process if the residual reached a specified set point can enhance the speed of convergence.

- Applying a denser mesh or allowing further iterations may enhance the resolution of the image.
- This technique can also be extended to 3D image reconstruction.
- Other optimization techniques can be applied to study the effect of each one and arrive at the best technique.

In addition to the fact that level set approach does promise to make an ill-posed problem better behaved, it offers other advantages such as:

- Performing numerical computations of a geometric object containing curves and surfaces on a fixed Cartesian grid without the need to parameterize such objects.
- The level set method has the ability to follow shapes with changing topology (i.e split in to multi-regions, develops holes or vice versa).
- The level set method does not require *a priori* assumption about the topology (i.e spatial location) nor the nature (i.e shape and size) of the inclusion.
- The level set method is well suited for high contrast image reconstruction with sharp boundaries. This is because the high contrast inclusion is incorporated explicitly in the level set model without it dominating the entire region and overshadowing the other low contrast inclusions. Unlike traditional regularization based techniques, which have the limitation of over smoothing the reconstructed image especially when a high contrast inclusion is dominating the region.

Because of such advantages, the level set method has a great potential for shape reconstruction applications and thus for multiphase image reconstruction.

6 Conclusion

The results in this paper demonstrate the potential and feasibility of the proposed level set technique for detecting, locating and characterizing all different phases possibly appearing in a multiphase process. Simulation and experimental results demonstrate a multi-phase level set based algorithm is capable of imaging three or four phase permittivity contrasts. Such promising results can also be extended to image more than 4 phases by adding more level set functions to the model accordingly. The nonlinear nature of the proposed algorithm as well as prior knowledge about the contrast permittivity values enabled us to recover those permittivity profiles by using one set of capacitance data. This is critically important in real life application where absolute ECT data can be used to recover multi-phase flow data without requiring a reference data. The hope is that the results of this paper will help in better understanding and further extension of the application of ECT for multi-phase flow imaging.

REFERENCES

[1] The Norwegian Society for Oil and Gas Measurement and The Norwegian Society of Chartered Technical and Scientific Professionals. “Handbook of multiphase flow metering,” March 2005.

[2] M. S. Beck and R. A. Williams, “Process tomography: a European innovation and its applications,” Meas. Sci. Technol., **vol 7**, pp 215–224, 1996.

[3] S. M. Huang, A. Plaskowski, C. G. Xie and M. S. Beck, "Capacitance-based tomographic flow imaging system," Electronics Letters, **vol. 24**, no, 7, pp 418–19, 1988.

[4] K. Brodowicz, L. Maryniak and T. Dyakowski, "Application of capacitance tomography for pneumatic conveying processes," in Proc. 1st ECAPT Conf. (European Concerted Action on Process Tomography), 1992, Manchester, March 26–29, 1992, ed. M S Beck, E Campogrande, M Morris, R A Williams and R C Waterfall (Southampton: Computational Mechanics) pp 361–8.

[5] G. E. Fasching and N. S. Smith, "A capacitive system for three- dimensional imaging of fluidized beds," Review of Scientific Instruments , **vol.62**, no.9, pp.2243,2251, Sep 1991.

[6] S.J. Wang, T. Dyakowski, C.G. Xie, R.A. Williams and M.S. Beck, "Real-time capacitance imaging of bubble formation at the distributor of a fluidized-bed," Chem. Eng. J. Biochem. Eng, **vol. 56**, no. 3, pp. 95–100, 1995.

[7] S. Liu, W. Q. Yang, H. G. Wang and Y. Su, "Investigation of square fluidized beds using capacitance tomography: preliminary results" Meas. Sci. Technol. **vol. 12**, no. 8, pp. 1120–5, 2001.

[8] R. He, C. M. Beck, R. C. Waterfall and M. S. Beck, "Applying capacitance tomography to combustion phenomena," Proc. 2nd ECAPT Conf. (European Concerted Action on Process Tomography), Karlsruhe, March 25–27, 1993 ed. M S Beck, E Campogrande, M Morris, R A Williams and R C Waterfall (Southampton: Comput Mechanics) pp 300–2.

[9] R. He, C. M. Beck, R. C. Waterfall and M. S. Beck, "Finite element modelling and experimental study of combustion phenomena using capacitance measurements," Proc. 3rd ECAPT Conf. (European Concerted Action on Process Tomography), Porto, March 24–26, 1994, pp 367–76.

[10] R. C. Waterfall, R. He, N. B. White and C. B. Beck, "Combustion imaging from electrical impedance measurements," Meas. Sci. Technol., **vol. 7**, pp. 369–74, 1996.

[11] R. White, "Using electrical capacitance tomography to monitor gas voids in a packed bed of solids," Measurement Science and Technology, **vol. 13**, no. 12, pp. 1842–1847, 2002.

[12] Ø. Isaksen, A. S. Dico and E. A. Hammer, "A capacitance based tomography system for interface measurement in separation vessels," Meas. Sci. Technol., **vol. 5**, pp. 1262–71, 1994.

[13] W. Q. Yang, M. S. Adam, R. Watson and M. S. Beck, "Monitoring water hammer by capacitance tomography," Electron. Lett., **vol. 32**, pp. 1778–9, 1996.

[14] W. Deabes, and M. Abdelrahman, "Solution of the forward problem of electric capacitance tomography of conductive materials," in The 13th World Multi- Conference on Systemics, Cybernetics and Informatics: WMSCI, Orlando, Florida, USA, 2009.

[15] E. AlHosani, M. Zhang and M. Soleimani, "A limited region electrical capacitance tomography for detection of deposits in pipelines," *IEEE Sensors Journal,* **vol. 15**, no. 11, pp. 6089-6099, 2015.

[16] L. A. Vese and T. F. Chan, "A Multiphase Level Set Framework for Image Segmentation Using the Mumford and Shah Model," *International Journal of Computer Vision,* **vol. 50**, no. 3, pp. 271–293, 2002.

[17] M. Soleimani and W. Lionheart, O. Dorn, "Level set reconstruction of conductivity and permittivity from boundary electrical measurements using experimental data," *Inverse Problems in Science and Engineering*, **vol. 14**, no. 2, pp. 193–210, 2006.

[18] S. Osher and J. A. Sethian, "Fronts Propagating with Curvature Dependent Speed: Algorithms Based on Hamilton-Jacobi Formulations," *Journal of Computational Physics,* **vol.79**, pp. 12-49, 1988.

[19] F. Santosa, "A level set approach for inverse problems involving obstacles ESAIM Control," *Optim. Calc. Variat.,* **vol. 1**, pp. 17–33, 1996.

[20] O. Dorn, E. L. Miller and C.M. Rappaport, "A shape reconstruction method for electromagnetic tomography using adjoint fields and level sets," *Inverse Problems*, **vol. 16**, pp. 1119-1156, 2000.

[21] A. Litman, D. Lesselier and F. Santosa, "Reconstruction of a two-dimensional binary obstacle by controlled evolution of a level-set," *Inverse Problems*, **vol. 14**, pp. 685-706, 1998.

[22] N. Irishina, D. Álvarez, O. Dorn and M. Moscoso, "Structural level set inversion for microwave breast screening," *Inverse Problems*, **vol. 26**, no. 3, 2010.

[23] M. Soleimani, O. Dorn, WRB Lionheart, "A narrow-band level set method applied to EIT in brain for cryosurgery monitoring," IEEE Transactions on Biomedical Engineering, vol. 53, no. 11, pp. 2257-2264, 2006.

List of Figures

Figure 1. The ECT system (a) schematic of the ECT system (b) ECT system of the University of Bath Engineering Tomography Lab.

Figure 2. The geometry of the variation of the point $\mathbf{r} \rightarrow \mathbf{r}'$ under a variation of $\boldsymbol{\psi}(\mathbf{r}) \rightarrow \boldsymbol{\psi}'(\mathbf{r})$

Figure 3. Employed level set representation for representing four different phases (i.e $\boldsymbol{\varepsilon_1}, \boldsymbol{\varepsilon_2}, \boldsymbol{\varepsilon_3}$ and $\boldsymbol{\varepsilon_4}$) by three level set functions.

Figure 4. Flowchart of the level set ECT image reconstruction algorithm developed for this study

Figure 5. Simulation results for case 1 (a) the true shape of the simulation (b) the reconstructed shape using level set method (c) the reconstructed shape using standard Tikhonov image reconstruction method

Figure 6. The norms of the error between the simulated and calculated capacitances for 250 iterations of the level set method for case 1.

Figure 7. a histogram of the permittivity distribution per pixel for case 1 (a) true shape, (b) the level set reconstruction, (c) the standard Tikhonov image reconstruction.

Figure 8. Simulation results for case 2 (a) the true shape of the simulation (b) the reconstructed shape using level set method (c) the reconstructed shape using standard Tikhonov image reconstruction method

Figure 9. The norms of the error between the simulated and calculated capacitances for 250 iterations of the level set method for case 2.

Figure10. A histogram of the permittivity distribution per pixel for case 2 (a) true shape, (b) the level set reconstruction, (c) the standard Tikhonov image reconstruction.

Figure 11. level set experimental results for case 3 (a) experimental setup 1, (b) experimental setup 2.

Figure 12. The norms of the error between the measured and calculated capacitances for 250 iterations of the level set method for case 3 (a) experimental setup 1, (b) setup 2.

Figure 13. a histogram of the permittivity distribution per pixel for case 3 (a) experimental setup 1, (b) experimental setup 2.

Figure 14. level set experimental results for case 4 (a) experimental setup 3, (b) experimental setup 4.

Figure 15. The norms of the error between the measured and calculated capacitances for 250 iterations of the level set method for case 4 (a) experimental setup 3, (b) setup 4.

Figure 16. a histogram of the permittivity distribution per pixel for case 4 (a) experimental setup 3, (b) experimental setup 4.

List of Tables

Table 1. A comparison between the true shape and the level set reconstruction in terms of the area fraction per phase for the simulated cases

Table 2. A comparison between the true shape and the level set reconstruction in terms of the area fraction per phase for the experimental cases